Article

Promoting Effect of Ultra-Fine Bubbles on CO$_2$ Hydrate Formation

Tsutomu Uchida [1,*] **, Hiroshi Miyoshi** [2] **, Kenji Yamazaki** [1] **and Kazutoshi Gohara** [1]

[1] Faculty of Engineering, Hokkaido University, Sapporo 060-8628, Japan; k-yamazaki@eng.hokudai.ac.jp (K.Y.); gohara@eng.hokudai.ac.jp (K.G.)

[2] Graduate School of Engineering, Hokkaido University, Sapporo 060-8628, Japan; miyo3941@icloud.com

* Correspondence: t-uchida@eng.hokudai.ac.jp; Tel.: +81-11-706-6635

Abstract: When gas hydrates dissociate into gas and liquid water, many gas bubbles form in the water. The large bubbles disappear after several minutes due to their buoyancy, while a large number of small bubbles (particularly sub-micron-order bubbles known as ultra-fine bubbles (UFBs)) remain in the water for a long time. In our previous studies, we demonstrated that the existence of UFBs is a major factor promoting gas hydrate formation. We then extended our research on this issue to carbon dioxide (CO$_2$) as it forms structure-I hydrates, similar to methane and ethane hydrates explored in previous studies; however, CO$_2$ saturated solutions present severe conditions for the survival of UFBs. The distribution measurements of CO$_2$ UFBs revealed that their average size was larger and number density was smaller than those of other hydrocarbon UFBs. Despite these conditions, the CO$_2$ hydrate formation tests confirmed that CO$_2$ UFBs played important roles in the expression of the promoting effect. The analysis showed that different UFB preparation processes resulted in different promoting effects. These findings can aid in better understanding the mechanism of the promoting (or memory) effect of gas hydrate formation.

Keywords: nanobubble; memory effect; carbon dioxide; induction time

1. Introduction

Methane hydrates existing below the deep seafloor are attracting significant attention as an unconventional natural gas resource, and many studies and developments have been conducted on this topic [1–4]. In the field of oil and gas development, gas hydrate research has focused on suppressing the formation and growth of gas hydrates, and this problem remains one of the main topics in gas hydrate research.

However, gas hydrates have unique properties, such as a large gas storage capacity; therefore, they are a promising medium for transporting and storing gases [5–7]. Additionally, gas hydrates, or more generally clathrate hydrates, have attracted attention as refrigerants owing to their melting points that are higher than that of ice [8–11], as they have a large latent heat similar to ice. Research on gas hydrate utilization has increased in recent years, and such research has focused on efficient gas hydrates formation.

Gas hydrates form from water and guest gases, which are stable under low-temperature and high-pressure conditions. Gas hydrate crystal formation requires relatively high supersaturation (or supercooling) conditions, similar to ice formation. Therefore, it is difficult to use gas hydrates in industry as the formation process is difficult to control and requires excess energy. Currently, the most promising approach to promoting the formation process is applying the "memory effect" phenomenon.

Under the memory effect, gas hydrate crystallization occurs under milder conditions than the initial formation conditions when its dissociated water is used. The mechanism of the memory effect remains unknown, and there are several hypotheses to explain it. One such hypothesis is the "water structuring hypothesis", which states that the fragments of the crystal lattice remain in the dissociated water, even after several hours, and act as the

nuclei of hydrate reformation [2,12–16]. This hypothesis is based on the concept that water has a hydrogen-bonding network. However, it has not yet been successful in experimentally verifying such structures or been proven. The other is the "gas dissolution hypothesis", which states that a sufficient number of guest molecules remain in the dissociated water and will shorten the dissolution of guest molecules during the reformation process [17]. As guest molecules are typically hydrophobic and have relatively low solubility in pure water, a large amount of gas must be dissolved into the liquid after it is consumed in the liquid. This process is a major barrier to crystallization. Although this hypothesis was proposed in a simulation study [17], Uchida et al. [18–20] demonstrated the existence of a large amount of ultra-fine bubbles (UFBs) in dissociated water, along with the memory effect expression of UFB-containing water without hydrate dissociation, which supported the "gas dissolution hypothesis".

UFBs are small gas bubbles with diameters of less than 1 μm [21] and unique properties, such as high internal pressure, low buoyancy, and the suppression of coalescence growth due to the presence of negative surface charges (ζ-potential). Based on these properties, UFBs are considered to have a long lifespan in liquids [22–24]. Our previous studies [18–20] confirmed that a large amount of UFB is formed in water when gas hydrate is dissociated. This process has also been supported by molecular dynamic simulations [25–27].

In our previous studies, we explored the expression of the memory effect (or promoting the phenomenon of gas hydrate formation) using hydrocarbon gases, such as methane (CH_4) [18], ethane (C_2H_6) [19], and propane (C_3H_8) [20], and demonstrated the promotion of gas hydrate formation, not only with hydrate-dissociated water, but also with the UFB-containing water prepared by an UFB generator without any hydrate dissociation processes. Based on these studies, UFBs are considered to play important roles in the hydrate memory effect. Carbon dioxide (CO_2) is a hydrate-forming greenhouse gas and can be separated and stored under deep-sea conditions to prevent its release into the atmosphere [28], or be injected into national gas hydrate layers for effective natural gas development [29]. CO_2 hydrate formation must be controlled if it is to be used in these industrial applications. Therefore, this study aims to experimentally verify the promoting effect of CO_2 UFBs on the hydrate formation process, which produces structure I-type hydrates, such as CH_4 and C_2H_6. However, the solubility of CO_2 in water is approximately two orders of magnitude higher than those of CH_4 and C_2H_6 [30]. Kondori et al. [27] demonstrated the size difference between CH_4 and CO_2 UFBs formed after hydrate dissociation. Additionally, solutions containing dissolved CO_2 have high acidity (low pH). As the high solubility and low pH are considered to significantly reduce the lifetime of UFBs, whether CO_2 UFBs contribute to the memory effect of CO_2 hydrates must be confirmed. The memory effect of CO_2 hydrate was previously demonstrated using ice-melted water [31]. As this supports the water structuring hypothesis, comparison with this study allows us to discuss the role of UFBs for expressing the memory effect.

2. Materials and Methods

2.1. Materials and UFB Measurements

We used three types of liquid samples to evaluate the effect of UFBs on the promotion of CO_2 hydrate formation, as used in our previous studies [18–20], including deionized pure water, hydrate-dissociated water prepared by dissolving CO_2 hydrate, and CO_2-UFB-containing water. Pure water was prepared by ion exchange (Essential Elix, Merck KGaA, Darmstadt, Germany), with a resistivity of approximately 15 MΩ cm. CO_2-hydrate-dissociated water was prepared by dissolving CO_2 hydrates (approximately 10 wt%) in pure water at room temperature (approximately 293 K). CO_2-UFB-containing water was generated using a micro-bubble generator (Aura tec, OM4-MDG-045) at 293 K by supplying CO_2 gas (99% in purity, Sankemi Co., Ltd., Hokkaido, Japan) for over 1 h. When using liquid samples for the CO_2 hydrate formation test, every liquid was verified to be transparent, indicating the complete disappearance of micro- or macroscopic bubbles.

We used both the light scattering technique and freeze-fractured replica observation using a transmission electron microscope (FFT) to characterize the CO_2 UFBs. The former includes two methods depending on the size of the UFBs. The number density (N) of UFBs with diameters larger than approximately 300 nm was measured by the laser-light scattering (LS) method. An argon-ion laser (λ = 514.5 nm) was introduced to the liquid sample in the glass cell (approximately 1 cm^3), and the bright spots (more than 20 UFBs in each sample, corresponding to $N > 10^6$ mL^{-1}) were measured using a CCD camera (Watec Co., Ltd., Yamagata, Japan, type WAT-232S) from the 90° direction. The particle-tracking analysis (PTA) method (MicrotracBEL, Co., Osaka, Japan, Zeta View) was used to measure smaller UFBs, which can measure both the particle size distributions (estimating N and average diameter D) and the ζ-potentials of UFBs with sizes of approximately 100 nm by tracking over 100 UFBs. The pH of the solution was measured using a pH sensor (Sato Keiryoki Mfg. Co., Ltd., Tokyo, Japan, type SK-620PHII). We followed the FFT method in our previous studies [18–20]; therefore, we have only briefly described it here. A small amount (less than 10 μL) of the liquid sample was quenched in liquid nitrogen, and set in the replication system (JEOL Ltd., Tokyo, Japan, type JFD-9010). The roughness of the freshly fractured surface (formed under approximately 150 K and 10^{-5} Pa conditions) was replicated by depositing platinum and carbon. The replica film was transferred onto a Cu-grid with a 43 × 43 μm opening and observed using a high-resolution transmission electron microscope (TEM: JEOL Ltd., Tokyo, Japan, type JEM-2010, accelerating voltage of 200 kV). Based on the image resolution of the imaging plate (Fujifilm Co., Tokyo, Japan, type FDL-UR-V) and noise from the surface roughness, we could identify UFBs with diameters ranging from several tens of nanometers to several microns. The existence of a UFB was verified by a hemispherical dent, while impurity appeared as convex protrusion. Therefore, this method allowed us to separately observe UFBs and other impurities. Over 200 UFBs were observed to obtain the size distribution and N in each liquid sample following the FFT method.

2.2. Promoting Effect of CO$_2$ Hydrate Formation Evaluation

We used the same system used in our previous study [19] for the CO_2 hydrate formation tests. A liquid sample (approximately 50 cm^3) was placed in a reaction vessel (232.2 cm^3), whose temperature was controlled by a cooling bath (274.2 ± 0.2 K). After purging the headspace with CO_2 gas, a test gas was introduced to the vessel at approximately 2.5 MPa. This experimental protocol was verified to remove the effect of gas contamination (such as air in the headspace of the vessel) on the hydrate formation results [19]. The gas hydrate formation test began with gentle agitation (approximately 300 rpm).

We measured the induction time to indicate the ease of CO_2 hydrate formation, which was defined as the time taken to reach the time of gas hydrate formation after reaching the equilibrium condition, as indicated by a sudden temperature increase or pressure drop. As the gas hydrate nucleation process is stochastic, we evaluated the nucleation probability distribution for ten repeated experiments. Significance was estimated using the Dunnett test (MS Excel 2010 and BellCurve) with at least 99% confidence ($p < 0.01$).

3. Results and Discussion

3.1. Characteristics of UFBs in Liquid Samples

Some of the liquid sample used for the hydrate formation experiment was used to analyze the characteristics of the UFBs contained within by three methods. The typical TEM images of the CO_2 UFBs in the CO_2-hydrate-dissociated water obtained following the FFT method are shown in Figure 1. Most of the UFBs were spherical or oval, and relatively larger than those observed in other gas UFBs [18–20]. We also observed a thin layer at the bubble surface (Figure 1b) or surrounding the bubble in the liquid phase (Figure 1c).
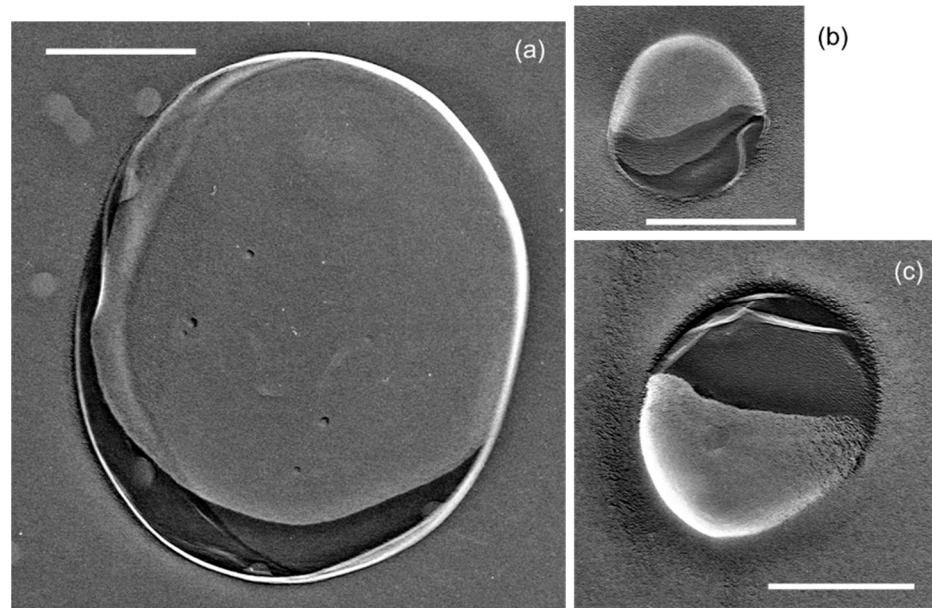
Figure 1. Typical TEM images of UFBs in the CO_2-hydrate-dissociation water. (**a**) Relatively large size UFB, (**b**) Normal size UFB with thin layer on the surface, (**c**) Normal size UFB surrounded by the liquid phase different from pure water. (scale bars: 300 nm).

Figure 2 shows the size distribution of the UFBs obtained by both the FFT and PTA methods from the same liquid sample. Table 1 shows the average diameter D and number density N of the CO_2 UFBs in each tested liquid sample. These figures and tables show that the CO_2 UFB in CO_2-hydrate-dissociated water exhibited a similar N value to other gas hydrate-dissociated water [18–20]. This is consistent with the finding that the D of CO_2 UFBs obtained by FFT was relatively larger than those observed in other gas hydrate systems. Although the N values measured by FFT and LS were similar, the values measured by the PTA method were two orders smaller than the others. This discrepancy could be because most of the UFBs were larger than several hundred nanometers (Figure 2), exceeding the measurable size of the PTA method. Therefore, we will conduct a quantitative comparison in the future.

Table 1. Average diameter D and number density N of UFBs in each liquid sample.

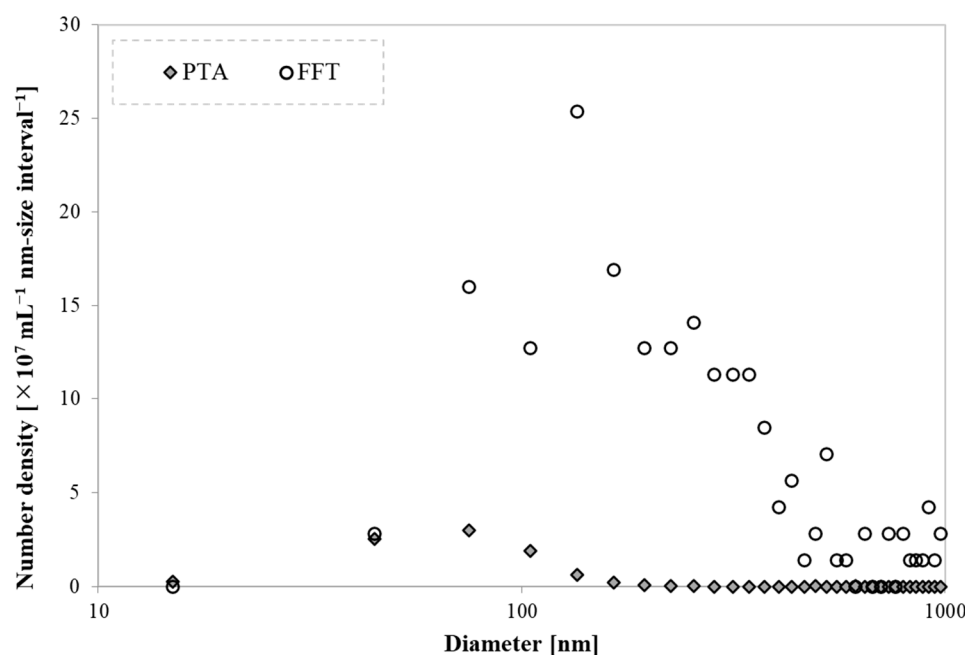| Sample	D (nm)	N ($\times 10^8$ mL^{-1})
CO$_2$-UFB-containing water	917 $\pm$ 443 (FFT) >300 (LS) 114 $\pm$ 21 (PTA)	8.1 $\pm$ 4.1 (FFT) 2.1 $\pm$ 0.7 (LS) 0.04 $\pm$ 0.01 (PTA)
CO$_2$-hydrate-dissociated water	672 $\pm$ 528 (FFT) >300 (LS) 81.7 $\pm$ 4.0 (PTA)	22.8 $\pm$ 7.1 (FFT) 2.0 $\pm$ 0.6 (LS) 0.087 (PTA)
	pH: 4.0	
	ζ-potential: -10.26 ± 5.3 [mV]	
pure water	N.A.	N.A.

Figure 2. CO_2 UFB distributions in hydrate dissociated water.

These results have important implications for the stability of CO_2 UFBs. The low pH value of 4.0 indicated that CO_2 was sufficiently dissolved in water. Therefore, the effect of contamination of gases other than CO_2 was considered negligible in this study. The ζ-potential of CO_2 UFBs exhibited a small absolute value of -10 mV, which was smaller than that of O_2 UFBs (-40 mV) under a pH of approximately 6.2 [32]. The relationship between the pH and ζ-potential is consistent with previous results reported by Takahashi [24]. Therefore, the smaller UFBs may tend to disappear by dissolving CO_2 molecules due to their higher internal pressure, and CO_2 UFBs are more likely to coalesce with one another due to their lower ζ-potential. Both effects would result in a larger average diameter. This is consistent with the finding that the CO_2 generator was required to operate for a longer time than those of other gases to form a sufficient number density of CO_2 UFBs.

3.2. CO_2 Hydrate Formation with Various Liquid Samples

Figure 3 shows the typical temperature profiles of CO_2 hydrate formation in the three types of liquid samples. After the vessel containing pressurized CO_2 was immersed in the cooling bath, the temperature decreased from room temperature to the set temperature of approximately 274.2 K. When the temperature reached equilibrium under the set pressure (approximately 279 K), the induction time began (shown as $t = 0$ in Figure 3). The duration until the sudden temperature increased due to CO_2 hydrate formation (indicated by the arrows in Figure 3) was taken as the induction time.

As shown in Figure 3, the formation of CO_2 hydrates began before the temperature reached the set temperature in CO_2-hydrate-dissociated (red solid line) and CO_2 UFB-containing water (green dotted line). However, in the formation experiment using pure water (blue dashed line), CO_2 hydrates formed after the temperature reached the set temperature. Therefore, it was confirmed that the induction time was shortened when using a liquid sample containing CO_2 UFBs, and the promoting effect was expressed.
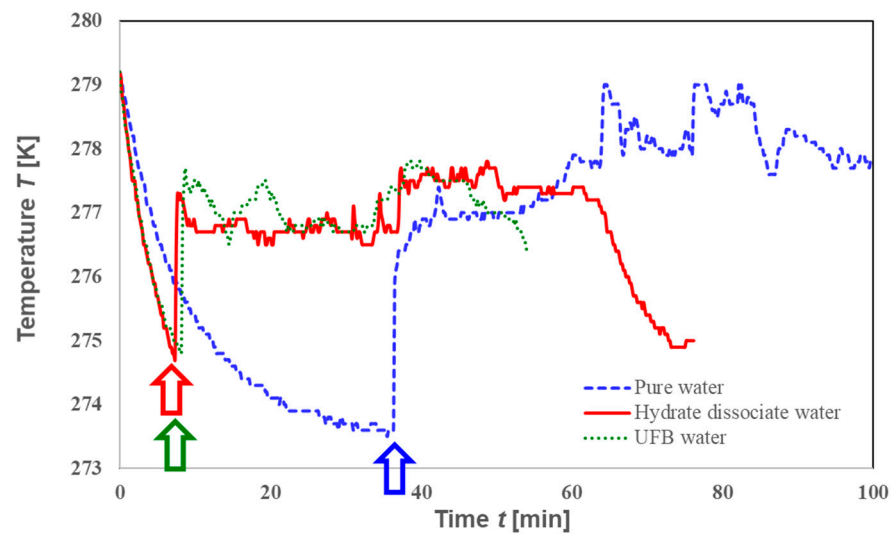
Figure 3. Temperature profile during hydrate formation (arrows indicate the formation points).

Another characteristic of CO_2 hydrate formation is that the reaction occurs in a cascade, rather than the two-step formation of C_2H_6 hydrate [19]. This would be due to the high solubility of CO_2 in water; therefore, even if dissolved CO_2 is consumed by hydrate formation, the amount of dissolved CO_2 did not sufficiently decrease to interrupt hydrate formation, and/or the dissolution rate from the gas phase was sufficiently fast.

3.3. Comparison of Memory Effects and Roles of UFBs

To explore the relationship between the probability nucleation rate and the induction time, formation experiments were repeatedly conducted to measure the induction time. Figure 4 shows the relationship between the probability nucleation rate of CO_2 hydrates $P(\tau)$ and the induction time τ obtained in this study.
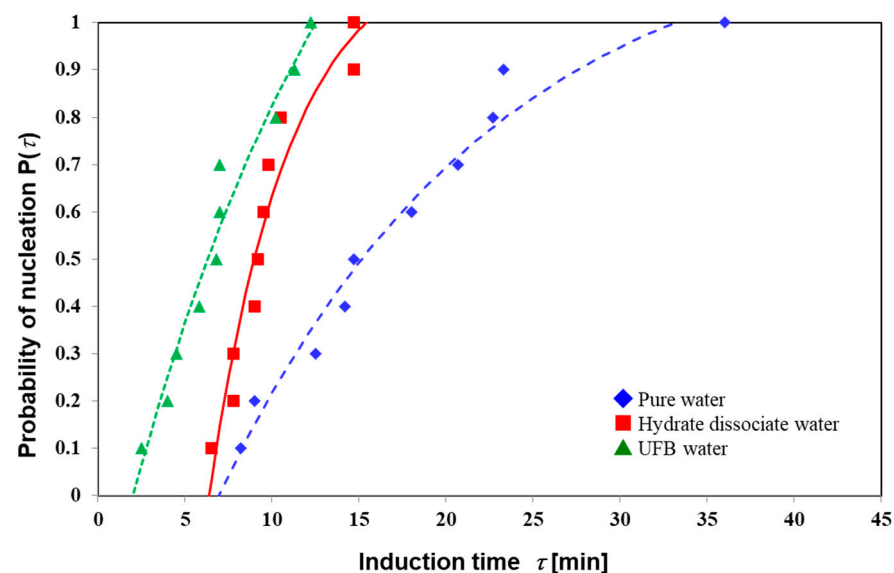

Figure 4. Probability of nucleation vs. induction time. Each point shows the experimental data (numerical data are available in Table A1) and each line shows the fitting curve of Equation (1).

This figure shows that both the nucleation probability curves of the CO_2-hydrate-dissociated (▲) and CO_2-UFB-containing water (■) were observed at a shorter induction time than that of pure water (♦). Again, it was confirmed that both types of liquid samples, including CO_2 UFBs, exhibited a memory effect. As CO_2-UFB-containing water did not

contain any hydrate structures, the guest dissolution hypothesis would be more appropriate for this CO_2 hydrate system than the water structuring hypothesis. This is the same conclusion as those drawn in our previous studies [18–20].

We then conducted a quantitative analysis of the promoting effect of CO_2 hydrate following a previous work [31]. Equation (1) was fitted to the probability of nucleation rate $(P(\tau))$ curves presented in Figure 4, and the fitting parameters of the nucleation frequency J and offset time τ_0 were examined.

$$P(\tau) = 1 - \exp\left[-J(\tau - \tau_0)\right], \tag{1}$$

As shown in Table 2, CO_2-hydrate-dissociated water had a promoting effect, such that τ_0 was lower than that of pure water, while J changed little. However, for CO_2-UFB-containing water, the promoting effect caused J to increase, although τ_0 remained almost the same. For the C_2H_6 hydrate, both the hydrate-dissociation and UFB-containing water exhibited a promoting effect by increasing J and decreasing τ_0 to the same extent. Therefore, the expression of the promoting effect of the CO_2 hydrate may differ slightly to that of hydrocarbon hydrates; that is, CO_2 UFBs promoted CO_2 hydrate formation; however, the mechanism differed between the preparation processes. Here, we discussed the nucleation probability with ten replicate experiments; however, more experiments are required for a detailed investigation [33]. Additionally, we only focused on the surface properties of the experimental materials (such as hydrophobic or hydrophilic) to consider the effect of fine surface bubbles on hydrate formation [34].

Table 2. Nucleation probability parameters.

Sample	τ_0 (min)	J ($\times 10^{-2}$ min^{-1})	$<\Delta t_{ind}>$ (min)
pure water	7.0 ± 0.7	6.3 ± 0.7	—
CO_2-UFB-contained water	6.4 ± 0.3	22 ± 0.8	8.0
CO_2-hydrate-dissociated water	2.0 ± 0.5	7.2 ± 5	11.3
pure water [31]	7.9	0.295	
meltwater [31]	58.8	2.29	

Compared to the parameters obtained to evaluate the freezing-memory effect [31], the value of J was much larger in this study, which could be due to the differences in hydrate formation, such as differences in the reaction systems with or without agitation. The expression pattern of the promoting effect with CO_2-UFB-containing water was qualitatively similar to that observed with meltwater, but differed to that observed with CO_2-saturated meltwater (similar to nitrogen-saturated meltwater) [31]. The reason for this discrepancy is unclear, but an additional number of experiments would provide a better understanding.

As in the previous study [19], we then compared the expected induction time $<\Delta t_{ind}>$ of the promoting effect with the difference in the area of the nucleation probability diagram (Figure 4). The magnitude of the promoting effect slightly differed between the CO_2-hydrate-dissociated and CO_2-UFB-containing water. The $<\Delta t_{ind}>$ value of CO_2-hydrate-dissociated water was approximately 1.4 times that of CO_2-UFB-containing water, as shown in the final column of Table 2. Compared to the case of C_2H_6 hydrate, in which the two $<\Delta t_{ind}>$ values were almost identical [19], this difference may be due to N, as CO_2 hydrates tend to nucleate at the gas–liquid interface [35]. However, Tables 1 and 2 show that the relationship between J and N was opposite. This novel insight into the promoting effect on CO_2 hydrate formation is discussed in the following paragraph.

As shown in Section 3.1, CO_2 UFBs have a relatively larger diameter and smaller number density than hydrocarbon gas UFBs [18–20], which is consistent with the low pH (approximately 4) of the solution containing CO_2 UFBs, as the low-pH condition could not prevent coalescence between the UFBs [24]. However, the CO_2 hydrate formation promoting effect were confirmed to be expressed in both CO_2-UFB-containing solutions. Therefore, we considered that CO_2 UFBs play important roles in the promoting effect of

CO_2 hydrate formation, despite their larger size and lower number density. The promoting mechanisms between the hydrate-dissociated water and UFB-containing water derived from the analysis of the nuclear probability curves differed, which is inconsistent with the results of previous works [18–20]. A possible cause of this difference is the difference in CO_2 saturation in water. Based on the preparation protocols, the UFB-containing water would be saturated with CO_2 even though CO_2 has high solubility. In contrast, the amount of CO_2 hydrate may be insufficient under the saturated conditions of hydrate-dissociated water.

As mentioned above, these parameters also differ to the memory effect observed with ice-melting water [31]. Therefore, we should also consider the terminology of 'memory' effect, which has been used as a general term for the formation-promoting phenomena. The mechanism of the promoting effect should also be considered when discussing the 'memory effect' of gas hydrate formation.

4. Conclusions

In this study, we investigated the relationship between the expression of the promoting effect and existence of UFBs using CO_2-hydrate-dissociated and CO_2-UFB-containing water. As CO_2 UFBs are generated under low-pH and high-solubility conditions, they tend to have smaller numbers (lower number density) and larger sizes (large average diameter) than other hydrocarbon UFBs. Nevertheless, the CO_2 hydrate formation induction time shortened for both liquid samples; thus, the promoting effect was confirmed to be expressed in the CO_2-UFB-containing system. These results support the gas dissolution hypothesis for memory effect mechanisms, rather than the water structuring hypothesis. Therefore, CO_2 UFBs would act as guest-molecule resources in the liquid phase. However, the analysis of the probability of nucleation rate curves suggested that CO_2 UFBs may exhibit different patterns for the promoting effect of CO_2 hydrates. This property is unique for CO_2 UFBs and is due to the high solubility of CO_2 in pure water.

Appendix A

Table A1. Numerical data for Figure 4.

Nucleation Probability	Induction Time (min)		
	Pure Water	CO$_2$ UFB-Containing Water	CO$_2$ Hydrate-Dissociated Water
0	7	6.4	2
0.1	8.2	6.5	2.5
0.2	9	7.8	4
0.3	12.5	7.8	4.5
0.4	14.2	9	5.8
0.5	14.7	9.2	6.8
0.6	18	9.5	7
0.7	20.7	9.8	7
0.8	22.7	10.5	10.2
0.9	23.3	14.7	11.3
1	36	14.7	12.2

References

1. Kvenvolden, K.A. Methane Hydrate—A major reservoir of carbon in the shallow geosphere? *Chem. Geol.* **1988**, *71*, 41–51. [CrossRef]
2. Sloan, E.D.; Koh, C.A. *Clathrate Hydrate of Natural Gases*, 3rd ed.; CRC Press: Boca Raton, FL, USA, 2007.
3. Masuda, Y.; Uchida, T.; Nagakubo, S.; Satoh, M. Methane hydrates. In *Fossil Fuels: Current Status and Future Directions, World Scientific Series in Current Energy Issues*; Crawley, G.M., Ed.; World Scientific Pub. Co. Pte. Ltd.: Singapore, 2016; Volume 1, Chapter 10; pp. 289–327.
4. Sloan, E.D. Fundamental principles and applications of natural gas hydrates. *Nature* **2004**, *426*, 353–363. [CrossRef] [PubMed]
5. Gudmundsson, J.; Borrehaug, A. Frozen hydrate for transport of natural gas. In Proceedings of the 2nd International Conference on Natural Gas Hydrates, Toulouse, France, 2–6 June 1996; pp. 415–422.
6. Gudmundsson, J.S.; Parlaktuna, M.; Levik, O.I.; Andresson, V. Laboratory for continuous production of natural gas hydrates. In Proceedings of the 5th International Conference on Natural Gas Hydrates, Trondheim, Norway, 13–16 June 2005; Tapir Academic Press: Trondheim, Norway, 2005; Volume 1, pp. 851–858.
7. Mimachi, H.; Takeya, S.; Yoneyama, A.; Hyodo, K.; Takeda, T.; Gotoh, Y.; Murayama, T. Natural gas storage and transportation within gas hydrate of smaller particle: Size dependence of self-preservation phenomenon of natural gas hydrate. *Chem. Eng. Sci.* **2014**, *118*, 208–213. [CrossRef]
8. Nakajimra, M.; Ohmura, R.; Mori, Y.H. Clathrate hydrate formation from cyclopentane-in-water emulsions. *Ind. Eng. Chem. Res.* **2008**, *47*, 8933–8939. [CrossRef]
9. Shimada, W.; Shiro, M.; Kondo, H.; Takeya, S.; Oyama, H.; Ebinuma, T.; Narita, H. Tetra-n-butyl ammonium bromide–water. *Acta Crystallogr. C Cryst. Struct. Commun.* **2005**, *61*, o65–o66. [CrossRef]
10. Lin, W.; Dalmazzone, D.; Fürst, W.; Delahaye, A.; Fournaison, L.; Clain, P. Accurate DSC measurement of the phase transition temperature in the TBPB—Water system. *J. Chem. Thermodyn.* **2013**, *61*, 132–137. [CrossRef]
11. Oshima, M.; Kida, M.; Nagao, J. Thermal and Crystallographic Properties of Tetra-n-butylammonium bromide + tetra-n-butylammonium chloride mixed semiclathrate hydrates. *J. Chem. Eng. Data* **2016**, *61*, 3334–3340. [CrossRef]
12. Parent, J.S.; Bishnoi, P.R. Investigation into the nucleation behavior of methane gas hydrates. *Chem. Eng. Commun.* **1996**, *144*, 51–64. [CrossRef]
13. Hwang, M.J.; Wright, D.A.; Kapur, A.; Holder, G.D. An experimental study of crystallization and crystal growth of methane hydrates from melting ice. *J. Inclusion Phenom. Molecul. Recogn. Chem.* **1990**, *8*, 103–116. [CrossRef]
14. Ohmura, R.; Ogawa, M.; Yasuoka, K.; Mori, Y.H. Statistical study of clathrate-hydrate nucleation in a water/hydrochlorofluorocarbon system: Search for the nature of the "memory effect". *J. Phys. Chem. B* **2003**, *107*, 5289–5293. [CrossRef]
15. Sefidroodi, H.; Abrahamsen, E.; Kelland, M.A. Investigation into the strength and source of the memory effect for cyclopentane hydrate. *Chem. Eng. Sci.* **2013**, *87*, 133–140. [CrossRef]
16. Buchanan, P.; Soper, A.K.; Thompson, H.; Westacott, R.E.; Creek, J.L.; Hubson, G.; Koh, C.A. Search for memory effects in methane hydrate: Structure of water before hydrate formation and after hydrate decomposition. *J. Chem. Phys.* **2005**, *123*, 164507. [CrossRef]
17. Rodger, P.M. Methane hydrate, melting and memory. *Ann. N. Y. Acad. Sci.* **2000**, *912*, 474–482. [CrossRef]
18. Uchida, T.; Yamazaki, K.; Gohara, K. Generation of micro- and nano-bubbles in water by dissociation of gas hydrates. *Korean J. Chem. Eng.* **2016**, *33*, 1749–1755. [CrossRef]
19. Uchida, T.; Yamazaki, K.; Gohara, K. Gas nano-bubbles as nucleation promoting in the gas-hydrate memory effect. *J. Phys. Chem. C* **2016**, *120*, 26620–26629. [CrossRef]
20. Uchida, T.; Miyoshi, H.; Sugibuchi, R.; Suzuta, A.; Yamazaki, K.; Gohara, K. Contribution of ultra-fine bubbles to promoting effect on propane hydrate formation. *Front. Chem.* **2020**, *8*, 480. [CrossRef] [PubMed]

21. ISO 20480-1: 2017 Fine Bubble Technology—General Principles for Usage and Measurement of Fine Bubbles—Part 1: Terminology. Available online: https://www.iso.org/obp/ui/#iso:std:iso:20480:-1:ed-1:v1:en (accessed on 14 April 2021).

22. Seddon, J.R.T.; Lohse, D.; Ducker, W.A.; Craig, V.S.J. A deliberation on nanobubbles at surfaces and in bulk. *ChemPhysChem* **2012**, *13*, 2179–2187. [CrossRef]

23. Oshita, S.; Uchida, T. Basic Characterization of nanobubbles and its potential applications. In *Bio-Nanotechnology: A Revolution in Biomedical Sciences, & Human Health*; Bagchi, D., Bagchi, M., Moriyama, H., Shahidi, F., Eds.; John Wiley & Sons, Ltd.: West Sussex, UK, 2013; Chapter 29; pp. 506–516.

24. Takahashi, M. ζ potential of microbubbles in aqueous solutions: Electrical properties of the gas-water interface. *J. Phys. Chem. B* **2005**, *109*, 21858–21864. [CrossRef]

25. Yagasaki, T.; Matsumoto, M.; Andoh, Y.; Okazaki, S.; Tanaka, H. Effect of bubble formation on the dissociation of methane hydrate in water: A molecular dynamic study. *J. Phys. Chem. B* **2014**, *118*, 1900–1906. [CrossRef]

26. Bagherzadeh, S.A.; Alavi, S.; Ripmeester, J.; Englezos, P. Formation of methane nano-bubbles during hydrate decomposition and their effect on hydrate growth. *J. Chem. Phys.* **2015**, *142*, 214701. [CrossRef]

27. Kondori, J.; James, L.; Zendehboudi, S. Molecular scale modeling approach to evaluate stability and dissociation of methane and carbon dioxide hydrates. *J. Mol. Liq.* **2020**, *297*, 111503. [CrossRef]

28. Zheng, J.; Chong, Z.R.; Qureshi, M.F.; Linga, P. Carbon dioxide sequestration via gas hydrates: A potential pathway toward decarbonization. *Energy Fuels* **2020**, *34*, 10529–10546. [CrossRef]

29. Castellani, B.; Rossetti, G.; Tupsakhare, S.; Rossi, F.; Nicolini, A.; Castaldi, M.J. Simulation of CO_2 storage and methane gas production from gas hydrates in a large scale laboratory reactor. *J. Petro. Sci. Eng.* **2016**, *147*, 515–527. [CrossRef]

30. The Chemical Society of Japan. *Kagaku-Binran (Handbook of Chemistry)*, 5th ed.; fundamental II-144-149; Maruzen Co. Ltd.: Tokyo, Japan, 2004.

31. Takeya, S.; Hori, A.; Hondoh, T.; Uchida, T. Freezing-memory effect of water on nucleation of CO_2 hydrate crystals. *J. Phys. Chem. B* **2000**, *104*, 4164–4168. [CrossRef]

32. May, E.F.; Wu, R.; Kelland, M.A.; Aman, Z.M.; Kozielski, K.A.; Hartley, P.G.; Maeda, N. Quantitative kinetic inhibitor comparisons and memory effect measurements from hydrate formation probability distributions. *Chem. Eng. Sci.* **2014**, *107*, 1–12. [CrossRef]

33. Huang, X.; Li, Z.; Deng, Y.; Cai, W.; Gu, L.; Lu, H. Effect of micro- and nanobubbles on the crystallization of THF hydrate based on the observation by atomic force microscopy. *J. Phys. Chem. C* **2020**, *124*, 13966–13975. [CrossRef]

34. Uchida, T.; Liu, S.; Enari, M.; Oshita, S.; Yamazaki, K.; Gohara, K. Effect of NaCl on the lifetime of micro- and nanobubbles. *Nanomaterials* **2016**, *6*, 31. [CrossRef] [PubMed]

35. Uchida, T.; Ebinuma, T.; Narita, H. Observations of CO_2-hydrate decomposition and reformation processes. *J. Cryst. Growth* **2000**, *217*, 189–200. [CrossRef]